

Hierarchical Task Control for Aerial Inspection

Àngel Santamaria-Navarro and Juan Andrade-Cetto

Abstract—This paper presents a task oriented control strategy for aerial vehicles equipped with a robotic arm and a camera attached to its end-effector. With this setting the camera can reach a new set of orientations previously not feasible for the quadrotor. The over-actuation of the whole system is exploited with a hierarchical control law to achieve a primary task consisting on a visual servoing control, whilst secondary tasks can also be attained to minimize gravitational effects or undesired arm configurations. Results are shown in a Robot Operating System (ROS) simulation.

I. INTRODUCTION

Unmanned aerial vehicles (UAVs), and in particular quadrotor systems, have gained popularity in the research community in recent years and are being used in a number of applications motivated by their significant increase in maneuverability, together with a decrease in weight and cost [1], [2], [3], [4], [5]. In all these cases, visual feedback plays an important role for the control of the platform.

Quadrotors are equipped with four aligned coplanar propellers. Due to their symmetric design, motion control is achieved by altering the rotation rate of one or more of these propellers, thereby changing its torque load and thrust lift characteristics. With this actuation technique, a quadrotor becomes an underactuated vehicle with only 4 DOF (3 linear and 1 angular controllable velocities as shown in Fig. 1(a)). This underactuation carries a limitation when an inspection task should be done.

By rigidly attaching the camera to a quadrotor, its field of view becomes limited by the 4 DOF of the quadrotor. To address underactuation, recent advances in UAV size-to-payload and manipulator weight-to-payload ratios suggest the possibility of attaching a manipulator arm to the base of the robot [6], [4]. In this work, we simulate the attachment of a serial arm to the quadrotor with a camera at its end effector (See Fig. 1(b)). Providing extra degrees of freedom to the camera allows to efficiently maneuver the platform during inspection tasks whilst maintaining the target on sight. This DOF redundancy is exploited not only to achieve a desired visual servo task, but to do so whilst attaining secondary tasks during the mission. In this paper, we use uncalibrated image-based visual servo [7] for the main control task, and secondary tasks that help keeping the platform stable.

Flying with a suspended load is a challenging task because the load significantly changes the flight characteristics of the aerial vehicle, and the stability of the vehicle-load system must be preserved. Therefore, it is essential that the flying

This work has been partially funded by the EU project ARCAS FP7-287617. The authors are with the Institut de Robòtica i Informàtica Industrial, CSIC-UPC, Llorens Artigas 4-6, Barcelona 08028, Spain, asantamaria, cetto@iri.upc.edu.

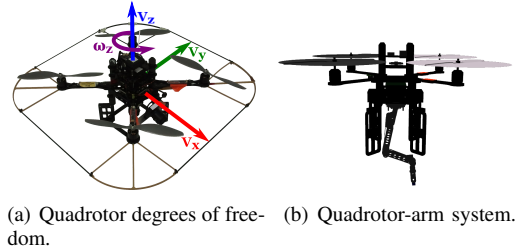


Fig. 1. The small UAV used in our simulations.

robot has the ability to minimize the effects of the arm on the flying system during the assigned maneuvers [8], [9].

The attached arm produces undesired dynamic effects to the quadrotor, such as the change of the center of mass during flight, that can be solved designing a low-level attitude controller such as a Cartesian impedance controller [10], or an adaptive controller [11]. To avoid this undesired behavior, the redundancy of the system in the form of extra DOFs could be exploited to develop a secondary stabilizing task after the primary servoing task. Other secondary tasks that can also be performed within a hierarchical framework, could be designed such as to optimize some given quality indices, e.g. manipulability, joint limits, etc., [12], [13].

The remainder of this article is structured as follows. In the next section a brief description of the image-based visual servo approach is explained. The quadrotor-arm robot model is given in Sec. 3. The task priority control of the over-actuated system is described in Sec. 4. Sec. 5 shows the feasibility of the proposed control strategy through simulation. Finally, conclusions are given in Sec. 6.

II. UNCALIBRATED IMAGE-BASED VISUAL SERVO

Drawing inspiration on [7], we can formulate the focal length in terms of the relation between the camera and target frames. To this end we set a reference system attached to the target object, and define a set of four control points as a basis for this reference system. Then, one can express the 3D coordinates of each target feature as a weighted sum of the elements of this basis. Computing the pose of the object with respect to the camera resorts to computing the location of these control points with respect to the camera frame. A least squares solution for the control point coordinates albeit scale, is given by the null eigenvector of a linear system made up of all 2D to 3D perspective projection relations between the target points. Given the fact that distances between control points must be preserved, these distance constraints can be used in a second least squares computation to solve for scale and focal length.

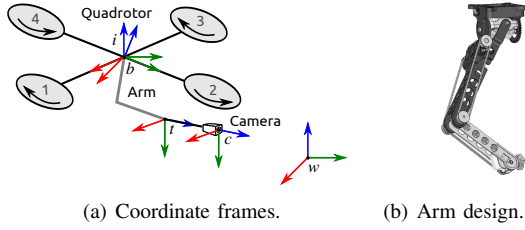


Fig. 2. Quadrotor-arm frame distribution and mechanical design of the 5DOF serial arm.

The aim of this image-based control schemes is to minimize the error $\mathbf{e}(t) = \mathbf{s}(t) - \mathbf{s}^*$, where $\mathbf{s}(t)$ are the current image coordinates of our set of target features, and \mathbf{s}^* are their final desired position in the image plane. If we select \mathbf{s} to be the projection of the control points, and disregarding the time variation of \mathbf{s}^* , the derivative of $\mathbf{e}(t)$ becomes $\dot{\mathbf{e}} = \dot{\mathbf{s}} = \mathbf{J}_{vs} \mathbf{v}_c$, with \mathbf{J}_{vs} corresponding to the calibration-free image Jacobian. Assuming an holonomic platform, the camera velocities \mathbf{v}_c can be used to command the robot with an exponential decoupled decrease of the error, i.e. $\dot{\mathbf{e}} = -\lambda \mathbf{e}$,

$$\mathbf{v}_c = -\lambda \mathbf{J}_{vs}^+ \mathbf{e}, \quad (1)$$

where \mathbf{J}_{vs}^+ is chosen as the Moore-Penrose pseudo-inverse of \mathbf{J}_{vs} , that is $\mathbf{J}_{vs}^+ = (\mathbf{J}_{vs}^T \mathbf{J}_{vs})^{-1} \mathbf{J}_{vs}^T$. For a more exhaustive explanation of this method for pose and focal length estimation we refer the reader to the above-mentioned paper.

III. ROBOT MODEL

A. Coordinate Frames

Consider the quadrotor-arm system equipped with a camera mounted on the arm's end-effector's as shown in Fig. 2(a). The goal is to servo the camera to a desired target, say for instance, a fiducial mark on an object to be inspected.

Without loss of generality, we consider the world frame w to be located at the target. We identify it with an ARTag marker attached to the object frame, and compute the location of the basis of the control points. At each iteration, the marker is detected in the scene, and the projection of the control points computed. With this, the position of the target with respect to the camera in c can be computed integrating the camera velocities obtained from the visual servo, and expressed as a homogeneous transform \mathbf{T}_c^w .

The quadrotor high-level controller commands velocities in the so-called inertial frame i , as shown in Fig. 2(a). This frame indicates the location of the vehicle w.r.t. w but rotated about the yaw axis. Both frames i and w have their x and y axes in parallel planes. The quadrotor, being an underactuated vehicle [14], has only 4 DOF, namely the linear velocities plus the yaw angular velocity ($v_{qx}, v_{qy}, v_{qz}, \omega_{qz}$) acting on this inertial frame. The low-level attitude controller moves the quadrotor body frame b to reach the desired velocities in i . Both frames i and b have the respective origins in the same point but a rotation about the roll and pitch angles exists between them.

Let $\mathbf{q}_a = [q_{a1}, \dots, q_{an}]^T$ be the n joint angles of the robotic arm attached to the vehicle. With the arm base frame

coincident with the quadrotor body frame b , the pose of the quadrotor ($x, y, z, \phi, \theta, \psi$) with respect to the target, is given by the concatenation of the homogenous transforms

$$\mathbf{T}_w^i = \mathbf{T}_b^i \mathbf{T}_t^b \mathbf{T}_c^t (\mathbf{T}_c^w)^{-1}, \quad (2)$$

with $\mathbf{T}_t^b(\mathbf{q}_a)$ corresponding to the arm kinematics.

We are in the position now to define a joint quadrotor-arm Jacobian that relates the local translational and angular velocities of the platform acting on the inertial frame and those of the n arm joints, $\mathbf{v}_{qa} = (v_{qx}, v_{qy}, v_{qz}, \omega_{qx}, \omega_{qy}, \omega_{qz}, \dot{q}_{a1}, \dots, \dot{q}_{an})^T$, to the desired camera velocities as computed from the visual servo

$$\mathbf{v}_c = \mathbf{J}_{qa} \mathbf{v}_{qa}, \quad (3)$$

with \mathbf{J}_{qa} the Jacobian matrix of the whole robot.

This velocity vector in the camera frame, can be expressed as a sum of the velocities added by the quadrotor movement and the arm kinematics (superscripts indicate the reference frame to make it clear to the reader)

$$\mathbf{v}_c^c = \mathbf{v}_q^c + \mathbf{v}_a^c, \quad (4)$$

where \mathbf{v}_a^c is obtained with the arm Jacobian \mathbf{J}_a .

$$\mathbf{v}_a^c = \begin{bmatrix} \mathbf{R}_b^c & \mathbf{0} \\ \mathbf{0} & \mathbf{R}_b^c \end{bmatrix} \mathbf{J}_a \dot{\mathbf{q}}_a = \bar{\mathbf{R}}_b^c \mathbf{J}_a \dot{\mathbf{q}}_a, \quad (5)$$

and where \mathbf{R}_b^c indicates the rotation of b with respect to c , and \mathbf{v}_q^c corresponds to the velocity of the quadrotor expressed in the c frame,

$$\mathbf{v}_q^c = \bar{\mathbf{R}}_b^c \begin{bmatrix} \mathbf{v}_q^b + \boldsymbol{\omega}_q^b \times \mathbf{r}_c^b \\ \boldsymbol{\omega}_q^b \end{bmatrix} = \begin{bmatrix} \mathbf{R}_b^c & \mathbf{R}_b^c [\mathbf{r}_c^b]^T \\ \mathbf{0} & \mathbf{R}_b^c \end{bmatrix} \mathbf{v}_q^b. \quad (6)$$

The term $\mathbf{r}_c^b(\mathbf{q}_a)$ indicates the vector between the b and c frames, i.e. the direct arm kinematics.

Finally, the velocity vector of the quadrotor in the body frame, \mathbf{v}_q^b , can be obtained using the quadrotor Jacobian \mathbf{J}_q formed by the rotation $\mathbf{R}(\phi, \theta)$ and the transfer matrix $\mathbf{T}(\phi, \theta)$ between the quadrotor inertial and body frames

$$\mathbf{v}_q^b = \mathbf{J}_q \mathbf{v}_q^i = \begin{bmatrix} \mathbf{R} & \mathbf{0}_{3 \times 3} \\ \mathbf{0}_{3 \times 3} & \mathbf{T} \end{bmatrix} \mathbf{v}_q^i, \quad (7)$$

where

$$\mathbf{R}(\phi, \theta) = \begin{bmatrix} c_\theta & s_\theta s_\phi & s_\theta c_\phi \\ 0 & c_\phi & -s_\phi \\ -s_\theta & c_\theta s_\phi & c_\theta c_\phi \end{bmatrix}, \mathbf{T}(\phi, \theta) = \begin{bmatrix} 1 & s_\phi t_\theta & c_\phi t_\theta \\ 0 & c_\phi & -s_\phi \\ 0 & s_\phi / c_\theta & c_\phi / c_\theta \end{bmatrix}, \quad (8)$$

and the notation $s_x = \sin(x)$, $c_x = \cos(x)$, $t_x = \tan(x)$. Combining Eqs. 1 and 3, we get

$$\mathbf{J}_{qa} \mathbf{v}_{qa} = -\lambda \mathbf{J}_{vs}^+ \mathbf{e}. \quad (9)$$

Due to quadrotor underactuation ([14]), its pitch and roll are internally controlled by the attitude subsystem and we cannot directly actuate them. So, to remove these variables from the control command, their contribution to the visual servo error can be isolated from that of the other control variables by extracting the columns of \mathbf{J}_{qa} and the rows of \mathbf{v}_{qa} corresponding to ω_{qx} and ω_{qy} , reading out these values

from the platform gyroscopes, and subtracting them from the camera velocity [15].

Rearranging terms

$$\mathbf{J}_{qa1} \dot{\mathbf{q}} = \underbrace{-\lambda \mathbf{J}_{vs}^+ \mathbf{e} - \mathbf{J}_{qa2}}_{\dot{\mathbf{q}}_1} \begin{bmatrix} \omega_{qx} \\ \omega_{qy} \end{bmatrix}, \quad (10)$$

where \mathbf{J}_{qa2} is the Jacobian formed by the columns of \mathbf{J}_{qa} corresponding to ω_{qx} and ω_{qy} , and \mathbf{J}_{qa1} is the Jacobian formed by all other columns of \mathbf{J}_{qa} , corresponding to the actuated variables $\dot{\mathbf{q}} = [v_{qx}, v_{qy}, v_{qz}, v_{qz}, \dot{q}_{a1}, \dots, \dot{q}_{an}]^T$.

With this, $\dot{\mathbf{q}}_1$ becomes our primary task velocity corresponding to the visual servo.

$$\dot{\mathbf{q}} = \mathbf{J}_{qa1}^+ \dot{\mathbf{q}}_1. \quad (11)$$

IV. HYERARCHICAL TASK PRIORITY CONTROL

The redundancy obtained with the arm's extra degrees of freedom can be exploited to achieve additional tasks acting on the null space of the quadrotor-arm Jacobian [16], while preserving the primary task in Eq. 11:

$$\dot{\mathbf{q}} = \mathbf{J}_{qa1}^+ \dot{\mathbf{q}}_1 + \mathbf{N}_{qa1} \dot{\mathbf{q}}_0, \quad (12)$$

where $\mathbf{N}_{qa1} = (\mathbf{I} - \mathbf{J}_{qa1}^+ \mathbf{J}_{qa1})$ is the null space projector for the main task. With this, the secondary task velocity $\dot{\mathbf{q}}_0$ will be used to reconfigure the robot structure without changing both the position and orientation of the end-effector (usually referred to as *internal motion*).

One possible way to specify the secondary task is to choose the velocity vector $\dot{\mathbf{q}}_0$ as the gradient of a scalar objective function to achieve some kind of optimization [13], [17]. With a more general approach, let $\boldsymbol{\sigma} = \mathbf{f}(\mathbf{q}) \in \mathbb{R}^m$ be the variables of a secondary task to be controlled, the following differential relationship holds:

$$\dot{\boldsymbol{\sigma}} = \frac{\partial \mathbf{f}(\mathbf{q})}{\partial \mathbf{q}} \dot{\mathbf{q}} = \mathbf{J}_\sigma(\mathbf{q}) \dot{\mathbf{q}}, \quad (13)$$

where $\mathbf{J}_\sigma(\mathbf{q}) \in \mathbb{R}^{m \times (4+n)}$ is the configuration-dependent task Jacobian.

Hence, by inverting Eq. 13 and by considering a regulation problem of $\boldsymbol{\sigma}$ to the desired value $\boldsymbol{\sigma}^*$, the following general solution can be employed

$$\dot{\mathbf{q}} = \mathbf{J}_{qa1}^+ \dot{\mathbf{q}}_1 + \mathbf{N}_{qa1} \mathbf{J}_\sigma^+ \boldsymbol{\Lambda}_\sigma \tilde{\boldsymbol{\sigma}}, \quad (14)$$

where $\boldsymbol{\Lambda}_\sigma \in \mathbb{R}^{m \times m}$ is a positive-definite matrix of gains, and $\tilde{\boldsymbol{\sigma}} = \boldsymbol{\sigma}^* - \boldsymbol{\sigma}$ is the task error.

Considering the high redundancy of the quadrotor-arm system, multiple secondary tasks can be arranged in hierarchy. As proposed in [18], the secondary objective function can be defined as a weighted sum of different objective sub-functions. However, the use of some of the sub-functions at the same time can produce undesired behaviors on the arm due to opposite effects of the sub-tasks. To deal with that and to avoid conservative stability conditions [19], the *augmented inverse-based projections method* is here considered [12]. In detail, the generic task is not projected onto the null space of the high hierarchy task, but onto the null space of the task

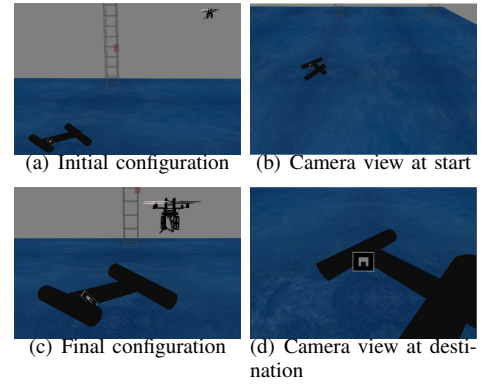


Fig. 3. ROS simulation of the proposed task priority visual servo for a quadrotor-arm system.

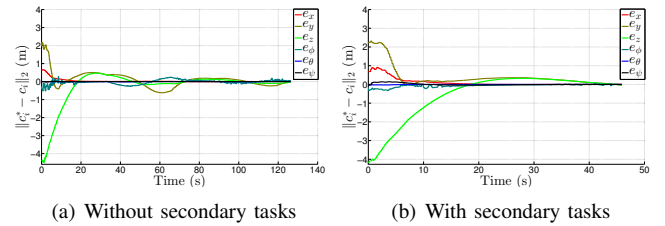


Fig. 4. Individual camera position and orientation error on each axis during the visual servo task.

achieved by considering the augmented Jacobian of all the higher hierarchy tasks.

In this work we consider two sub-tasks: 1) center of gravity control, 2) joint-limit avoidance. By denoting with \mathbf{J}_G and \mathbf{J}_L the Jacobian matrices for the center of gravity and for the joint-limit avoidance control, respectively, where the priority of the task follows the previous enumerating order, the desired system velocity can be rewritten as follows,

$$\dot{\mathbf{q}} = \mathbf{J}_{qa1}^+ \dot{\mathbf{q}}_1 + \mathbf{N}_{qa1} \mathbf{J}_G^+ \tilde{\boldsymbol{\sigma}}_G + \mathbf{N}_{qa1|G} \mathbf{J}_L^+ \tilde{\boldsymbol{\sigma}}_L, \quad (15)$$

with $\mathbf{N}_{qa1|G}$, the joint projector of the primary task and of the center of gravity secondary task, which is defined as

$$\mathbf{N}_{qa1|G} = (\mathbf{I} - \mathbf{J}_{qa1|G}^+ \mathbf{J}_{qa1|G}), \quad (16)$$

and $\mathbf{J}_{qa1|G}$ represents the augmented Jacobian

$$\mathbf{J}_{qa1|G} = \begin{bmatrix} \mathbf{J}_{qa1} \\ \mathbf{J}_G \end{bmatrix}. \quad (17)$$

The explicit derivation of the subtask Jacobians (\mathbf{J}_G and \mathbf{J}_L) as well as the variables to be controlled ($\tilde{\boldsymbol{\sigma}}_G$ and $\tilde{\boldsymbol{\sigma}}_L$) is not included due to space limitations. The reader is welcome to contact the main author for further details.

V. EXPERIMENTS

By attaching a 5DOF arm to the quadrotor we end up with a 9 DOF overactuated system. The robotic arm was designed with a joint setting to compensate the possible noise existing in the quadrotor positioning, i.e. to maintain the target in a fixed position w.r.t. the camera frame whilst the quadrotor is hovering still but subject to external perturbations. We present now simulations in ROS for a dynamical model of

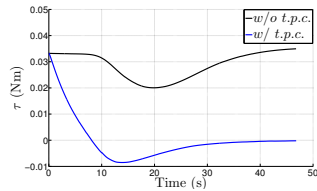


Fig. 5. Torque in the quadrotor produced by the arm during visual servoing task with and without task priority control.

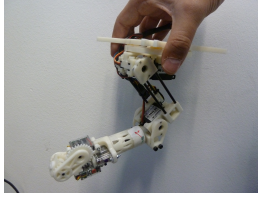


Fig. 6. First prototype of a very-light weight robotic arm. This is work in progress.

an Asctec Pelican quadrotor. The arm design is shown in Fig 2(b).

The quadrotor-arm system is teleoperated to an initial position as shown in Fig. 3 (a-c). At that point, the visual servo method is switched on, together with the secondary tasks. Fig. 3 (d-f) show the final robot configuration and how the arm changed its joint values to reach the desired camera location. Previous servo implementations for take off and landing consider only targets parallel to the quadrotor horizontal plane and do not compromise flight stability [7]. With the proposed over-actuated system, there are no restrictions on the target orientation that can compromise flight stability.

We first simulate a servo scheme to show the effect of adding the secondary tasks. Fig. 4 shows the camera pose error during the servoing task (i.e. $e_i = \|c_i^* - c_i\|_2$ with c_i^* and c_i the individual desired and current pose terms $i = [x, y, z, \phi, \theta, \psi]$). Note the difference in time scale. Whilst both servo schemes reach the target, the use of the secondary tasks produces a more efficient controller. This is due to the undesired torque added to the quadrotor when the weight distribution of the arm is not aligned along the quadrotor CoG. By the addition of the secondary tasks, this torque is reduced as shown in Fig. 5 during the servoing task. So, flight stability can be enhanced by the correct parametrization of the sub-tasks and therefore the time to reach the target.

VI. CONCLUSIONS

We have presented a task priority control scheme for aerial inspection. A serial arm is attached to the base of a quadrotor, and a camera is fixed at its end-effector. A primary task is designed to respond to visual servo control commands. The presented control law takes into account the hierarchy of the tasks by projecting each one into the Jacobian null space of the previous one. The technique is demonstrated in a ROS simulation, and we are currently working on the implementation of the system in a real robot setting. Fig. 6

shows a snapshot of our first prototype for a very-light weight UAV robotic arm.

ACKNOWLEDGMENT

The authors would like to thank P. Grosch (pgrosch@iri.upc.edu) from Workshop-IRI for his assistance and support on the real arm setting design and construction.

REFERENCES

- [1] L. Marconi, F. Basile, G. Caprari, R. Carloni, P. Chiacchio, C. Hurzeler, V. Lippiello, R. Naldi, J. Nikolic, B. Siciliano, S. Stramigioli, and E. Zwicker, "Aerial service robotics: The airobots perspective," in *Proc. 2th Int. Conf. App. Rob. Pow. Ind.*, Zurich, Sep. 2012, pp. 64–69.
- [2] D. Mellinger, Q. Lindsey, M. Shomin, and V. Kumar, "Design, modeling, estimation and control for aerial grasping and manipulation," in *Proc. IEEE/RSJ Int. Conf. Intell. Robots Syst.*, San Francisco, Sep. 2011, pp. 2668–2673.
- [3] A. Ollero and K. Kondak, "10 years in the cooperation of unnamed aerial systems," in *Proc. IEEE/RSJ Int. Conf. Intell. Robots Syst.*, Vilamoura, Oct. 2012, pp. 5450–5451.
- [4] M. Orsag, C. Korpela, and P. Oh, "Modeling and control of MM-UAV: Mobile manipulating unmanned aerial vehicle," *J. Int. Robotic Syst.*, vol. 69, no. 1-4, pp. 227–240, 2013.
- [5] P. Pounds, D. Bersak, and A. Dollar, "Grasping from the air: Hovering capture and load stability," in *Proc. IEEE Int. Conf. Robotics Autom.*, Shanghai, May 2011, pp. 2491–2498.
- [6] C. Korpela, T. Danko, and P. Oh, "Designing a system for mobile manipulation from an unmanned aerial vehicle," in *Proc. IEEE Int. Conf. Tech. Pract. Rob. App.*, 2011, pp. 109–114.
- [7] A. Santamaria-Navarro and J. Andrade-Cetto, "Uncalibrated image-based visual servoing," in *Proc. IEEE Int. Conf. Robotics Autom.*, Karlsruhe, May 2013, pp. 5247–5252.
- [8] C. Korpela, M. Orsag, T. Danko, B. Kobe, C. McNeil, R. Pisch, and P. Oh, "Flight stability in aerial redundant manipulators," in *Proc. IEEE Int. Conf. Robotics Autom.*, Saint Paul, May 2012, pp. 3529–3530.
- [9] I. Palunko, P. Cruz, and R. Fierro, "Agile load transportation: Safe and efficient load manipulation with aerial robots," *Robotics Autom. Mag.*, vol. 19, no. 3, pp. 69–79, 2012.
- [10] V. Lippiello and F. Ruggiero, "Exploiting redundancy in Cartesian impedance control of UAVs equipped with a robotic arm," in *Proc. IEEE/RSJ Int. Conf. Intell. Robots Syst.*, Vilamoura, Oct. 2012, pp. 3768–3773.
- [11] G. Antonelli, E. Cataldi, P. Giordano, S. Chiaverini, and A. Franchi, "Experimental validation of a new adaptive control scheme for quadrotors mavs," in *Proc. IEEE/RSJ Int. Conf. Intell. Robots Syst.*, Tokyo, Nov. 2013, pp. 2439–2444.
- [12] P. Baerlocher and R. Boulic, "Task-priority formulations for the kinematic control of highly redundant articulated structures," *J. Int. Robotic Syst.*, vol. 1, pp. 323–329, 1998.
- [13] S. Chiaverini, "Singularity-robust task-priority redundancy resolution for real-time kinematic control of robot manipulators," *IEEE Trans. Robotics Autom.*, vol. 13, no. 3, pp. 398–410, 1997.
- [14] T. Hamel and R. Mahony, "Image based visual servo control for a class of aerial robotic systems," *Automatica*, vol. 43, no. 11, pp. 1975–1983, 2007.
- [15] R. Mahony, V. Kumar, and P. Corke, "Multirotor aerial vehicles: Modeling, estimation, and control of quadrotor," *Robotics Autom. Mag.*, vol. 19, no. 3, pp. 20–32, 2012.
- [16] Y. Nakamura, H. Hanafusa, and T. Yoshikawa, "Task-priority based redundancy control of robot manipulators," *Int. J. Robotics Res.*, vol. 6, no. 2, pp. 3–15, 1987.
- [17] Y. Nakamura, *Advanced Robotics: Redundancy and Optimization*. Addison-Wesley, 1990.
- [18] V. Lippiello, R. Mebarki, and F. Ruggiero, "Visual coordinated landing of a UAV on a mobile robot manipulator," in *Proc. 11th*, Linkoping, Oct. 2013, pp. 1–7.
- [19] G. Antonelli, "Stability analysis for prioritized closed-loop inverse kinematic algorithms for redundant robotic systems," *IEEE Trans. Robotics*, vol. 25, no. 5, pp. 985–994, 2009.